arXiv:0804.2520v2 [nlin.CD] 26 Aug 2008

Topology of Chaotic Mixing Patterns

Jean-Luc Thiffeault*

Department of Mathematics, University of Wisconsin, Madison, WI 53706, USA

Matthew D. Finn

School of Mathematical Sciences, University of Adelaide, Adelaide SA 5005, Australia

Emmanuelle Gouillart

Unité mixte Saint-Gobain/CNRS "Surface du Verre et Interfaces,"
39 quai Lucien Lefranc, 93303 Aubervilliers Cedex, France

Toby Hall

Department of Mathematical Sciences,
University of Liverpool, Liverpool L69 7ZL, UK

(Dated: August 27, 2008)

A stirring device consisting of a periodic motion of rods induces a mapping of the fluid domain to itself, which can be regarded as a homeomorphism of a punctured surface. Having the rods undergo a topologically-complex motion guarantees at least a minimum amount of stretching of material lines, which is important for chaotic mixing. We use topological considerations to describe the nature of the injection of unmixed material into a central mixing region, which takes place at *injection cusps*. A topological index formula allow us to predict the possible types of unstable foliations that can arise for a fixed number of rods.

Keywords: chaotic advection, stirring and mixing, topological chaos, viscous flows

By stirring a fluid, mixing is greatly enhanced. By this we mean that if our goal is to homogenise the concentration of a substance, such as milk in a teacup, then a spoon is an effective way to mix. But in many industrial applications, such as food and polymer processing, the fluid is very viscous, so that stirring is difficult and costly. Hence, insight into the types of stirring that lead to good mixing is valuable. We explain how the mixing pattern — the characteristic shape traced out by a blob of dye after a few stirring periods — is tightly connected with topological properties of the stirring motion. In particular, we can enumerate the allowable number of pathways where material gets injected into the mixing region, as a function of the number of stirring rods.

*Electronic address: jeanluc@mailaps.org

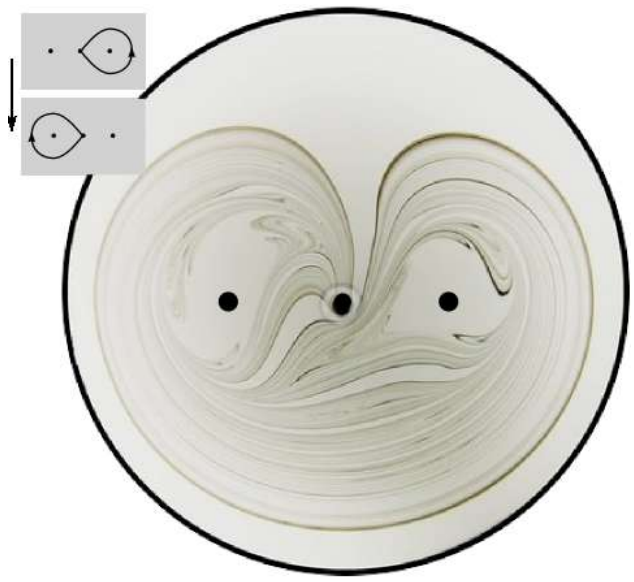

FIG. 1: The figure-eight stirring protocol. The inset shows the sequence of rod motions. The central black circle is the stirring rod, and the other two circles locate the position of regular islands, which serve as 'ghost rods.' (Experiments by E. Gouillart and O. Dauchot, CEA Saclay [1].)

I. STIRRING WITH RODS

A *rod stirring device*, where a number of rods are moved around in a fluid, is the most natural and intuitive method of stirring. The number of rods, their shape, and the nature of their motion constitute a *stirring protocol*. For example, Fig. 1 shows the result of stirring with the *figure-eight* protocol, whereby a single rod in a closed vessel traces a lemniscate shape. The Reynolds number is very small, so that the fluid (sugar syrup) is in the Stokes regime, where inertial forces are negligible and pressure and viscous forces are in balance. Because of the shape of the rod and container, three-dimensional effects are negligible. The fluid is the pale background, and a blob of black ink has been stretched by a few periods of the rod motion. The evident filamentation of the blob is characteristic of *chaotic advection* [2, 3], which greatly enhances mixing effectiveness in viscous flows.

We aim to understand the features of rod stirring protocols such as those depicted in Figs. 1, 2, and 3 from topological considerations. The new topological features that we discuss can be divided in two broad categories: (i) The injection cusps and their role; (ii) The identification of higher-pronged singularities directly in flow simulations. Though both of these concepts are familiar from the topological study of surface homeomorphisms [4, 5], we interpret them here in light of practical stirring protocols. Our study is a natural continuation of the original investigation by Boyland *et al.* [6] and the subsequent work of Gouillart *et al.* [1]. Our goal is to refine the previous approaches by looking for more detailed features of the Thurston–Nielsen classification in real fluid flows.

As an illustration, we examine the topological features visible in Fig. 1. The two unmixed regions in the centre of the loops of the figure-eight play the role of two extra rods, called *ghost rods* [7], so that we can regard this protocol as effectively involving three rods. Three rods is the minimum needed to guarantee exponential stretching of material lines [6, 8], and

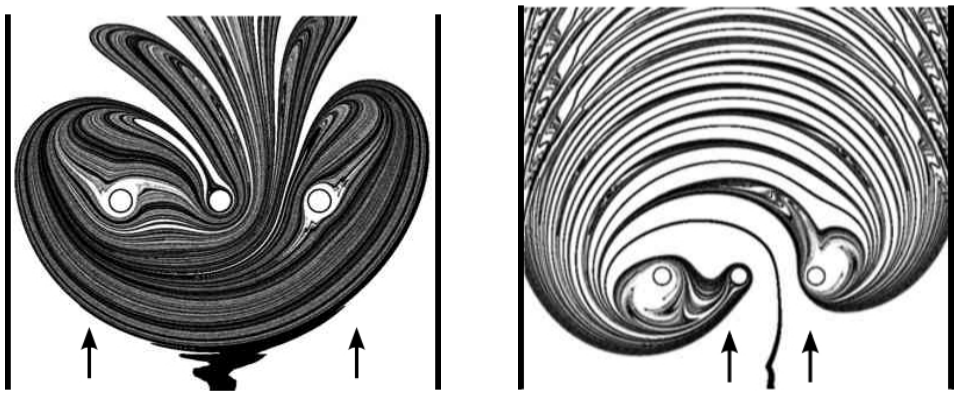

(a) (b)

FIG. 2: Numerical simulations of flow in a channel with a figure-eight rod stirring protocol. (a) Injection cusp against flow; (b) Injection cusp facing flow. The flow direction is from the bottom to the top of the figures.

for the figure-eight protocol the length of material lines grows by at least a factor of $(1+\sqrt{2})^2$ at each period. This is the first feature that can be understood from the topology of the rod motion: it places a lower bound on the *topological entropy*, which is closely related to the rate of stretching of material lines in two dimensions. This aspect has been well studied [6, 7, 8, 9, 10, 11, 12, 13, 14, 15, 16, 17].

Less well studied is another crucial feature obvious in Fig. 1: the unmixed fluid (white) is injected into the mixing region (kidney-shaped darker region) from the top part of the region, where a cusp is clearly visible. We say that the figure-eight protocol has one *injection cusp*. In fact, for three rods the situation in Fig. 1 is typical; for instance, a kidney-shaped mixing region is also evident in the efficient stirring protocol of Boyland *et al.* [6]. The nature of the injection of unmixed material into the central region has a profound impact on mixing rates, as was shown in recent experiments [1]. In these experiments the rate of injection of unmixed material into the central region of a stirring device dramatically limited the efficiency of mixing. This injection took place along injection cusps as described here, hence the number of injection cusps and their positions are clearly important for mixing.

The importance of injection cusps is even more apparent when dealing with *open flows*. Open flows, as opposed to flows in closed vessels, involve fluid that enters and subsequently exits a mixing region. This situtation is very common in industrial settings, since it allows continuous operation without the need to empty the vessel. Typical fluid particles only remain in the mixing region for a short time. Figure 2 shows the figure-eight stirring protocols in an open channel. The only difference between cases (a) and (b) is the direction of rotation of the rods. In a closed vessel, reversing the direction of rotation merely moves the injection cusp from top to bottom, but in an open flow it moves the injection cusp either facing the flow or against it. In Fig. 2(a), the injection cusp is downstream, so the passive scalar enters the mixing region from behind. This is clear from the dye filament at the bottom, which skirts the mixing region from the right. In contrast, Fig. 2(b) shows the opposite case, where the injection cusp is upstream. In that case the dye is drawn directly into the mixing region. Clearly these two cases have radically different mixing properties, as evidenced by the different dye patterns downstream. Thus, being able to predict the number

and nature of injection cusps from the rod motion is of crucial importance. The qualitative details of Fig. 2 are independent of the manner in which dye is injected. The extra injection cusps visible downstream in Fig. 2(a) are an artifact of the open-flow configuration: they are images of the single injection cusp being advected downstream by the mean flow at each period. The results presented in the rest of the paper apply rigorously only to closed flows, but it is evident from Fig. 2 that many qualitative features carry over from closed to open flows.

In this paper we will see that the number and position of injection cusps depends on the topology of the rod motion. The number of injection cusps will depend on the number of rods (or ghost rods), but for a fixed number of rods only a few configurations are possible. This is because the number of injection cusps is constrained by a topological *index formula*. Jana *et al.* [18] studied the impact of the topology of streamlines on chaotic advection. They used the Euler–Poincare–Hopf formula (see Section III) to determine the allowable fixed-point structure of steady velocity fields. When the flow is time-dependent, instantaneous fixed points of the velocity field mean little for chaotic advection (except when the time dependence is weak). Our study addresses arbitrary time-periodic flows by studying the mapping of fluid elements (the Lagrangian map) directly, from a topological perpective.

The paper is organised as follows. In Section II we present some necessary mathematical background, in particular the idea of *pseudo-Anosov* stirring protocols. We identify mathematical objects such as the *unstable foliation* in a specific fluid-dynamical example. The unstable foliation associated with a pseudo-Anosov protocol is the central object of our study. In Section III we use a topological index formula to enumerate the possible unstable foliations for a given number of stirring rods, and Section IV is devoted to a stirring device that exhibits a *hyperbolic* injection cusp, that is a cusp associated with the unstable manifold of a hyperbolic orbit. Such a cusp is less obviously identifiable from flow visualization, but can still be inferred by examining the topological properties of the stirring protocol. Finally, we summarise and discuss our work in Section V.

II. PSEUDO-ANOSOV STIRRING PROTOCOLS

In this section we will translate the physical system — a stirring protocol — into objects suitable for mathematical study. As mentioned in Section I, our focus will be on very viscous flows, where stirring and mixing is challenging, and we consider the flow to be essentially two-dimensional, as is typical of shallow or stratified flows. In these circumstances, a periodic motion of rods leads to a periodic velocity field. (Note that the rods may end up permuted amongst themselves at the end of each period.) This velocity field will induce a motion of fluid elements from their position at the beginning of a period to a new position at the end. Crucially, the fluid elements do not necessarily return to the same position — if they did, this would be a very poor stirring protocol indeed!

A periodic stirring protocol in a two-dimensional flow thus induces a *homeomorphism* φ from a surface $\mathcal{S}$ to itself. A homeomorphism is an invertible continuous map whose inverse is also continuous. In our case, φ describes the mapping of fluid elements after one full period of stirring, obtained from solving the Stokes equation, and $\mathcal{S}$ is the *disc* with holes (or *punctures*) in it, corresponding to rods. We treat rods as infinitesimal punctures (see Fig. 4(c)), since topologically this makes no difference. As a special case, rods that remain fixed are often called *baffles*. Topologically speaking, moving rods and fixed baffles are the same: they are holes in the surface $\mathcal{S}$. However, the homeomorphism φ acts on them

differently: the moving rods can be permuted, whilst the fixed baffles remain in place. Here, we shall not make a distinction between stirring rods and fixed baffles, and refer to both as stirring rods. Hence, a few stirring rods may be fixed by some stirring protocols, such as the figure-eight protocol in Fig. 1 which fixes two rods (the islands, or ghost rods). The outer boundary of the disc is invariant under φ, corresponding to the no-slip boundary condition.

Our task is to categorise all possible φ that lead to good mixing. This requires defining both what we mean by 'categorise' and 'good mixing.' The categorisation will be done up to isotopy, which is a way of defining the topological equivalence of homeomorphisms. Two homeomorphisms φ and ψ are *isotopic* if ψ can be continuously 'reached' from φ without moving the rods. If we imagine the two-dimensional fluid as a rubber sheet, this means that the two configurations attained by the sheet after application of either φ or ψ are the same, up to deformation of the sheet. In that case, we write $\varphi \simeq \psi$. Obviously, topology is unconcerned by hydrodynamic details and only deals with coarse properties of the homeomorphisms.

To pursue the categorisation, we invoke the Thurston–Nielsen (TN) classification theorem [4, 5], which describes the range of possible behaviour of a homeomorphism φ. Specifically, the theorem says that φ is isotopic to a homeomorphism φ', where φ' is either *finite-order*, *reducible*, or *pseudo-Anosov*. These three cases give the *isotopy class* of φ, and φ' is called the TN representative of the isotopy class. Finite-order means that φ' is periodic (that is, φ'^m = identity for some integer $m > 0$), and this cannot give good mixing since it implies nearby fluid elements will periodically come back near each other. The reducible case implies there are regions of fluid that remain invariant under φ', which again is terrible for mixing since there are then regions that do not mix with each other. For both finite-order and reducible φ', the actual homeomorphism φ could in practice exhibit much more complicated properties than φ', but this cannot be inferred by the rod motion itself. In the viscous flows that we have studied, φ and φ' appear to have similar properties.

The third case, when φ' is pseudo-Anosov (or pA), is both the most interesting mathematically and most relevant for mixing. In fact, we will define 'good mixing' as φ' having the pA property. Mathematically, a pA homeomorphism φ' leaves invariant a transverse pair of measured singular foliations, $(\mathcal{F}^{\mathrm{u}}, \mu^{\mathrm{u}})$ and $(\mathcal{F}^{\mathrm{s}}, \mu^{\mathrm{s}})$, such that $\varphi'(\mathcal{F}^{\mathrm{u}}, \mu^{\mathrm{u}}) = (\mathcal{F}^{\mathrm{u}}, \lambda\,\mu^{\mathrm{u}})$ and $\varphi'(\mathcal{F}^{\mathrm{s}}, \mu^{\mathrm{s}}) = (\mathcal{F}^{\mathrm{s}}, \lambda^{-1}\mu^{\mathrm{s}})$, for *dilatation* $\lambda > 1$. (The logarithm of the dilatation is the *topological entropy*.) Here μ^{u} and μ^{s} are the transverse measures for their respective foliation. There are several terms that need explaining in this definition, and we will illustrate what they mean by an example.

Figure 3 shows the result of a numerical simulation of a two-dimensional viscous (Stokes) flow. The container is circular, and the fluid is stirred with four rods, shown aligned horizontally in the centre. (The velocity field for these simulations was determined using a fast spectrally-accurate complex variable method [11], and the particle advection computed with a high-order Runge–Kutta scheme.) The inset illustrates the motion of the stirring rods: they are successively interchanged with their neighbour, in the direction shown. This protocol is written $\sigma_1\sigma_2\sigma_3^{-1}$, where σ_i denotes the clockwise interchange of rod i with rod $(i+1)$, and σ_i^{-1} its anticlockwise counterpart [6, 12, 19]. Thus, σ_i^{-1} is the inverse operation to σ_i. The subscript i in $\sigma_i^{\pm 1}$ refers to the physical position of a rod from left to right, and does not label a specific rod. The collection $\sigma_i^{\pm 1}$, $i = 1, \ldots, n-1$, generates the *braid group* on n strands. We apply the $\sigma_i^{\pm 1}$ operations, called *braid group generators*, in temporal order from left to right. Repeated generators are written as powers, as in $\sigma_i\sigma_i = \sigma_i^2$. This sequence of generators, called a *braid word*, defines our stirring protocol, which gives us the homeomor-

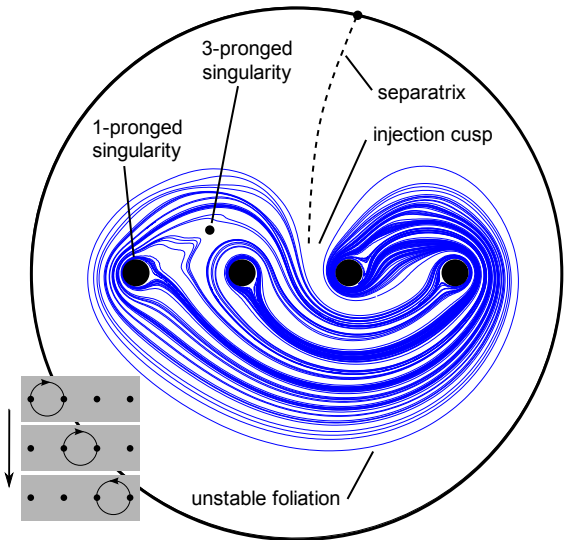

FIG. 3: Numerical simulation of the four-rod periodic stirring protocol $\sigma_1\sigma_2\sigma_3^{-1}$ in a viscous flow, corresponding to three rod interchanges for each period (inset). This sequence of interchanges forces the flow to be isotopic to a pseudo-Anosov homeomorphism. A material line advected for six periods reveals leaves of the unstable foliation $\mathcal{F}^{\mathrm{u}}$. The foliation exhibits four 1-pronged singularities around the rods, one interior 3-pronged singularity (in the region indicated by a dot, between and just above the first and second rods), and a separatrix attached to the disc's outer boundary, visible as an injection cusp along from the top into the mixing region. (The position of the singularities and separatrix are approximate.) Compare with Fig. 4, which shows typical leaves of the foliation in the neighbourhood of singularities.

TABLE I: The pseudo-Anosov stirring protocols used in this paper, defined in terms of braid group generators. The generator σ_i denotes the clockwise interchange of rod i with rod $(i+1)$, and σ_i^{-1} its anticlockwise counterpart, where i indicates the physical position of a rod in the sequence from left to right. The generators are read from left to right in time.

punctures	protocol	injection cusps	figure
3	$\sigma_2^{-2}\,\sigma_1^2$	1	Fig. 1, the figure-eight protocol
4	$\sigma_1\sigma_2\sigma_3^{-1}$	1	Fig. 3
4	$\sigma_1\sigma_2^{-1}\sigma_3\sigma_2^{-1}$	2	Fig. 5(a)
5	$\sigma_1\sigma_2^{-1}\sigma_3\sigma_4^{-1}\sigma_3\sigma_2^{-1}$	3	Fig. 5(b)
5	$\sigma_1\sigma_2\sigma_3\sigma_2^3\sigma_3^2\sigma_4\sigma_2\sigma_3\sigma_2^3$	1	Fig. 7

phism φ after we solve the Stokes equations for a viscous fluid. Table I defines the protocols used in this paper in terms of braid group generators.

The homeomorphism φ, by the Thurston–Nielsen theorem, is isotopic to the TN representative φ', which is pseudo-Anosov in this case. Remarkably, in viscous flows there is often very little visual difference between the action of φ and φ', and we find many features of φ' reflected directly in Fig. 3. This need not be the case in general: the dynamics of φ is at least as complicated as that of φ', in a precise sense [6, 20, 21], but can in practice be

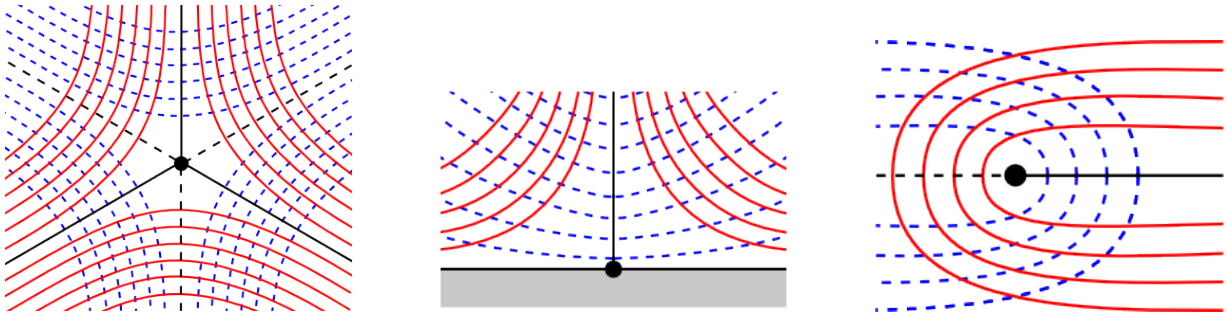

FIG. 4: For the unstable foliation $\mathcal{F}^{\mathrm{u}}$ and stable foliation $\mathcal{F}^{\mathrm{s}}$: (a) The neighbourhood of a 3-pronged singularity; typical leaves of $\mathcal{F}^{\mathrm{u}}$ are shown as solid lines, dashed lines for those of $\mathcal{F}^{\mathrm{s}}$. (b) The neighbourhood of a boundary singularity. A separatrix of $\mathcal{F}^{\mathrm{u}}$ emanates from the singularity, and separatrices for $\mathcal{F}^{\mathrm{u}}$ and $\mathcal{F}^{\mathrm{s}}$ alternate around the boundary. (c) We regard a rod as an infinitesimal point (or puncture), corresponding to a 1-pronged singularity. The leaves of the foliations fold and meet at separatrices attached to the rod.

considerably more so.

The folded lines in the background of Fig. 3 are a small material closed loop that was evolved for six full periods of the stirring protocol. As the material line is evolved for more and more periods, it converges to the unstable foliation, tracing out $\mathcal{F}^{\mathrm{u}}$ and allowing us to visualise it as a striated pattern. (The stable foliation $\mathcal{F}^{\mathrm{s}}$ is invisible in such experiments, so we shall not have much use for it here.) That the foliation $\mathcal{F}^{\mathrm{u}}$ remains invariant under φ' means that at each application of φ' the bundle of lines in Fig. 3 is unchanged, except for the lines getting denser: each application multiplies the number of lines in a given region by λ, the dilatation. (A local count of the line density is what the invariant measure μ^{u} gives us.) The unstable foliation $\mathcal{F}^{\mathrm{u}}$ is thus the object that captures the essence of stretching and folding in a chaotic flow.

Finally, the 'pseudo' in pseudo-Anosov is tied to the 'singular' in singular foliation. An Anosov homeomorphism, such as Arnold's cat map [22], can only exist on surfaces of zero Euler characteristic such as the torus. This is because the torus is a surface on which a nonvanishing vector field (in this case the foliation) can be smoothly combed. For other surfaces, such as our punctured disc, the best one can do is to comb the foliation and leave some singularities. Three such singularities are shown in Fig. 4. The singularities are characterised by the number of *prongs* associated with them. The prongs are separatrices, emanating from the singular point, around which the foliation branches. For instance, Fig. 4(a) shows a 3-pronged singularity: the leaves of the unstable foliation $\mathcal{F}^{\mathrm{u}}$ (solid lines) branch around the singularity in a triangular pattern around three separatrices. The dashed lines show leaves of the stable foliation, $\mathcal{F}^{\mathrm{s}}$. Figure 4(b) shows a separatrix of $\mathcal{F}^{\mathrm{u}}$ attached to the outer boundary of the disc at a singularity. Unstable and stable separatrices alternate around the boundary. Figure 4(c) shows a 1-pronged singularity, which occurs around rods, as we will see below.

The stirring device in Fig. 3 shows a total of six singularities in $\mathcal{F}^{\mathrm{u}}$. Most obviously, there is a 1-pronged singularity around each of the four rods, because the leaves are folded around each rod and meet at a separatrix, as in Fig. 4(c). Next, there is a 3-pronged singularity, in

the region marked with a dot in the picture (this dot is not a rod). That the singularity has three separatrices is evident if one tries to extend the foliation near the singularity: three bundles of leaves will meet at a point, which must then be a singularity. Finally, there is a separatrix connected to the disc's outer boundary at a singularity, as in Fig. 4(b), though this is not as easy to see. From Fig. 4(b) we expect that a boundary singularity will be manifested as a cusp in $\mathcal{F}^{\mathrm{u}}$, a consequence of the separatrix emanating from the boundary, and leading to injection of material into the mixing region (Fig. 3).

In the pA case, almost every aspect of the Thurston–Nielsen classification theorem can thus be identified directly in Fig. 3. Rods and the outer boundary possess singularities, and often other (interior) singularities arise in the flow itself, such as the 3-pronged singularity indicated by a dot in Fig. 3. We will refer to singularities not associated with rods or the outer boundary as *interior singularities*. Our reference protocol of Fig. 3 demonstrates that the unstable foliation $\mathcal{F}^{\mathrm{u}}$ and its singularities embody many important features of the underlying flow. We shall thus take the unstable foliation as the central focus of our study.

III. SINGULARITIES OF THE FOLIATION

An unstable foliation must satisfy three rules if it is to support a stirring protocol corresponding to a pseudo-Anosov homeomorphisms [23]:

1. Every stirring rod (or ghost rod, such as the islands in the figure-eight protocol) must be enclosed in a 1-pronged singularity (Fig. 4(c)). This is a physical requirement: 1-pronged singularities are the mathematical consequence of physical stirring, since the unstable foliation wraps around the rod. A rod enclosed in a higher-pronged singularity makes the rod irrelevant to stirring, since the singularity would exist regardless of the rod. Hence, we disregard this possibility.

2. The outer boundary of the disc contains at least one separatrix of $\mathcal{F}^{\mathrm{u}}$, as in Fig. 4(b). The number of separatrices on the outer boundary corresponds to the number of injection cusps into the mixing region.

3. The smallest number of prongs an interior singularity can have is 3. This is because 2-pronged singularities are just regular points (they are not 'true' singularities of the foliation), and pseudo-Anosovs do not have 1-pronged singularities away from punctures and boundary components.

We will use these three rules to limit the number of allowable *singularity data* of the unstable foliation $\mathcal{F}^{\mathrm{u}}$. The singularity data of a foliation $\mathcal{F}$ is the sequence $(N_{\mathrm{sep}}, N_3, N_4, \ldots)$, where N_{sep} is the number of separatrices on the outer boundary, and N_p is the number of interior p-pronged singularities for each $p \geq 3$. To enumerate the possible distinct singularity data of the unstable foliation for n rods, we use a standard *index formula*, which relates the nature of the singularities to a topological invariant, the *Euler characteristic* of the disc,

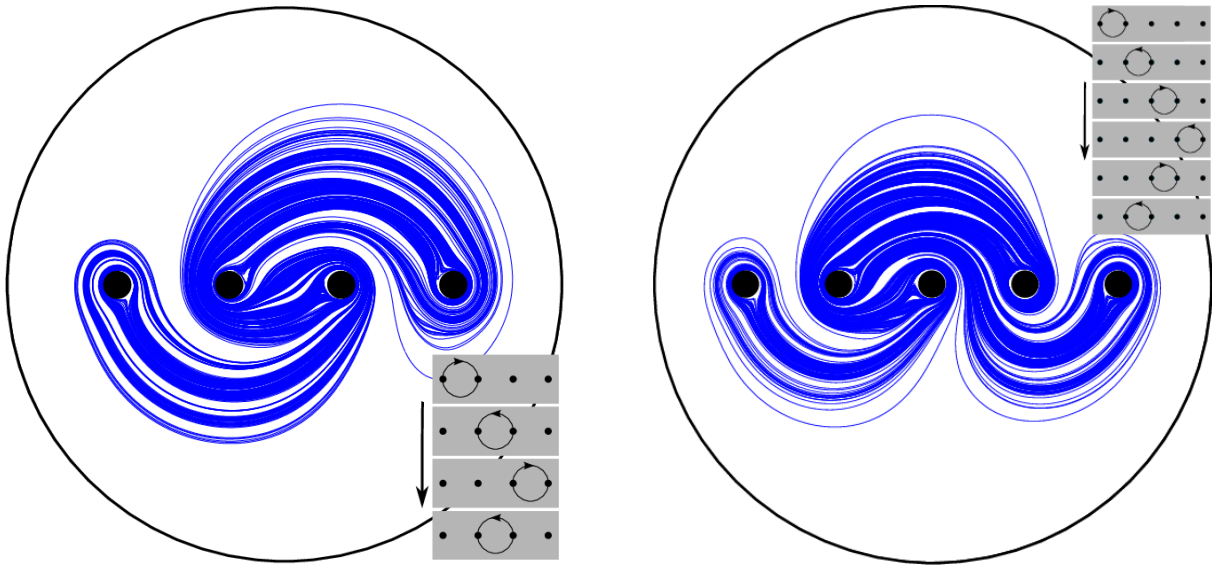

(a) (b)

FIG. 5: Numerical simulations of (a) the stirring protocol $\sigma_1\sigma_2^{-1}\sigma_3\sigma_2^{-1}$ for 4 rods, with two injection cusps; (b) the stirring protocol $\sigma_1\sigma_2^{-1}\sigma_3\sigma_4^{-1}\sigma_3\sigma_2^{-1}$ for 5 rods, with three injection cusps.

$\chi_{\text{disc}} = 1$.[1] This index formula says that

$$n - N_{\text{sep}} - \sum_{p\geq 3}(p-2)N_p = 2\chi_{\text{disc}} = 2. \tag{1}$$

Formula (1) is a well-known extension to foliations of the classical Euler–Poincaré–Hopf formula for vector fields [25, 26] (see for example page 1352 of [24, p. 1352]). It is important to note that the only positive contribution to the left hand side of (1) is the term n, the number of rods. Hence if there is a large number of rods, there must either be a large number of singularities and boundary separatrices, or a small number of singularities some of which have many prongs.

In order for (1) to be satisfied, the boundary separatrices and interior singularities must contribute $(2-n)$ to the left hand side. For $n = 3$, the only possibility is to have a single separatrix on the boundary. There is therefore unique singularity data for three stirring rods in a disc, corresponding to the kidney-shaped region in Fig. 1: the separatrix on the boundary corresponds to a single injection cusp into the mixing region.

For $n = 4$, the boundary separatrices and interior singularities must contribute -2 to the left hand side of (1), which means that there must either be two separatrices on the boundary, or one separatrix on the boundary and an interior 3-pronged singularity. These two cases correspond to the unstable foliations of the second and third protocols in Table I, as depicted in Figs. 5(a) and 3.

[1] More generally, the Euler characteristic of a surface of genus g with b boundaries is $2-2g-b$, where the genus is the number of 'handles' attached to a sphere. In particular, $\chi_{\text{sphere}} = 2$, $\chi_{\text{disc}} = 2-1 = 1$, and $\chi_{\text{torus}} = 2 - 2\cdot 1 = 0$.

TABLE II: The allowable singularity data $(N_{\rm sep}, N_3, N_4, \ldots)$ for n rods. Each rod has a 1-pronged singularity, and formula (1) must be satisfied. $N_{\rm sep}$ gives the number of separatrices on the outer boundary, and N_p gives the number of p-pronged interior singularities.

n	$N_{\rm sep}$	N_3	N_4	N_5
3	1			
4	2	0		
4	1	1		
5	3	0	0	
5	2	1	0	
5	1	2	0	
5	1	0	1	
6	4	0	0	0
6	3	1	0	0
6	2	2	0	0
6	2	0	1	0
6	1	3	0	0
6	1	1	1	0
6	1	0	0	1

As we add more rods, there are more possibilities for the singularity data. For example, Fig. 5(b) shows a protocol for five rods ($n = 5$) with three boundary separatrices ($N_{\rm sep} = 3$), corresponding to three injection cusps, and no interior singularities.

The maximum number of interior singularities occurs when there is a single boundary separatrix. The rods and this separatrix then contribute $n - 1$ to the left hand side of (1), and so (1) can be satisfied if there are $n - 3$ interior 3-pronged singularities. That is, the maximum possible number of interior singularities occurs for $N_3 = n-3$. On the other hand, in order to have no interior singularities it is necessary to have $n - 2$ boundary separatrices. This corresponds to the maximum possible number of injection cusps into the stirring region.

Table II provides a complete summary of the allowable singularity data for the first few values of n. The number of possible distinct singularity data for a foliation increases sharply with the number of rods n, as is evident in Fig. 6 (solid line). A convenient expression for the number of singularity data is

$$\#\text{ of singularity data} = \sum_{k=0}^{n-3} \mathfrak{p}(k) \tag{2}$$

where $\mathfrak{p}(k)$ is a *partition function* [27]. The partition function counts how many distinct ways positive integers can sum to k, with $\mathfrak{p}(0)$ defined as 1:

$$\mathfrak{p}(k) = \#\text{ of elements in the set } \Big\{ S \subseteq \mathbb{Z}^+ \,:\, \sum_{i \in S} i = k \Big\}. \tag{3}$$

The partition function has no simple exact closed form. To find the asymptotic form of (2) for large n, we can use the Hardy–Ramanujan asymptotic form for $\mathfrak{p}(k)$, and replace the

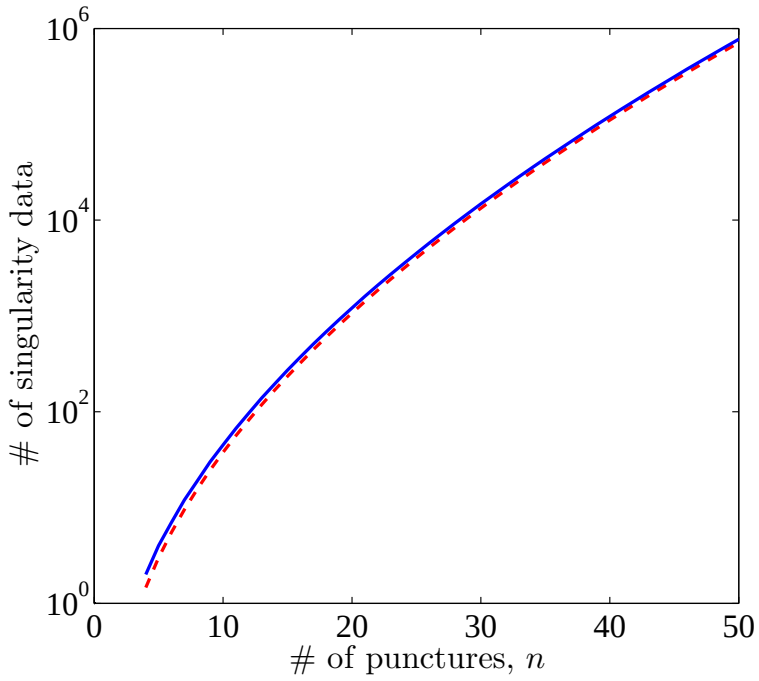

FIG. 6: The number of distinct singularity data increases rapidly with the number of punctures (or rods). The solid line is exact and is obtained by summing partition functions as in (2); the dashed line is the asymptotic form (4).

sum by an integral, to get

$$\#\text{ of singularity data} \sim \frac{1}{2\pi\sqrt{2\,(n-3)}}\exp\left(\pi\sqrt{2(n-3)/3}\right), \qquad n \gg 1. \tag{4}$$

The dashed line in Fig. 6 shows that the aymptotic form captures the correct order of magnitude for large n.

IV. HYPERBOLIC INJECTION CUSPS

Injection cusps are not always as plainly visible as in the cases presented thus far. However, as we will see in this section, their presence can still be inferred by examining the topological properties of the rod motion, including if necessary the motion of ghost rods. This section also helps to clarify the type of topological information that can be gleaned from the motion of rods [7, 15, 28]:

- If the motion of the rods themselves forms a pseudo-Anosov braid, then the rod motion yields interesting topological information even with no knowledge of ghost rods. This is the case with all the protocols in the paper thus far (except the figure-eight, which involves two obvious ghost rods). The topological information is then "robust," in the sense that it does not depend on the specific hydrodynamics of the fluid.

- If the motion of the rods does not imply a pseudo-Anosov, such as when there is only one or two rods [6], and chaotic behaviour is observed regardless, then ghost rods must

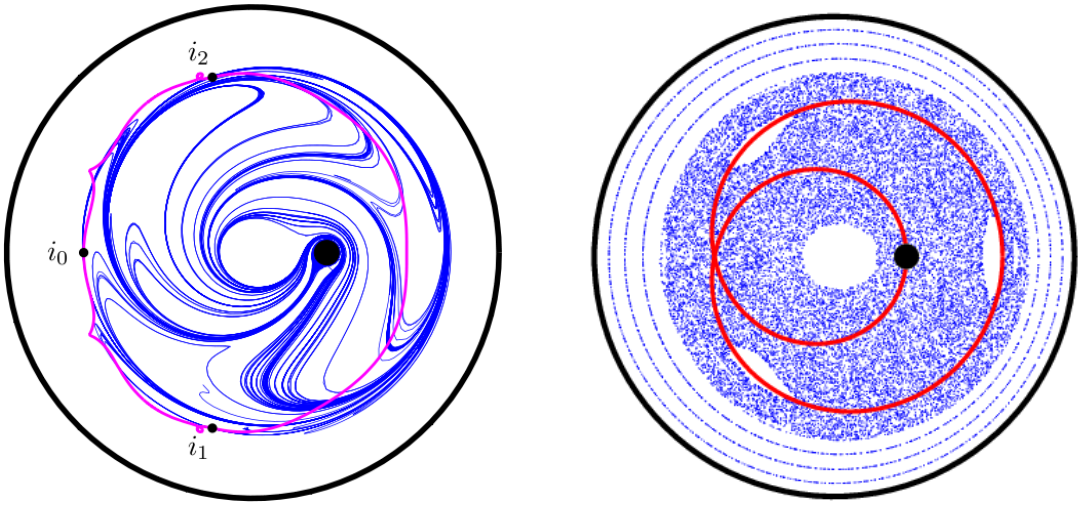

(a) (b)

FIG. 7: (a) Numerical simulation of a single rod tracing out an epitrochoidal path [solid line in (b)] stretching a material line for 7 periods. The period-3 orbit discussed in the text is shown superimposed, with iterates i_0, i_1, and i_2. (b) A Poincaré section (stroboscopic map) of some representative trajectories shows that the phase space consists of a large chaotic region and several regions of regular behaviour.

be included. This means either looking for regular islands (as in the example in this section) or for unstable periodic orbits. However, the presence and location of such periodic structures depend on the specific hydrodynamic model (here Stokes flow for a viscous fluid).

The protocol discussed in the present section is of the latter type. Figure 7(a) shows a material line advected by a one-rod stirring device, where the rod follows an epitrochoidal path. The path of the rod is shown as a solid line in Fig. 7(b), superimposed on a Poincaré section. We make two observations about Fig. 7: (i) The Poincaré section reveals a mixed phase space, consisting of a large chaotic region and several smaller regular regions, including a regular region that completely encloses the wall. (ii) The injection cusps into the mixing region are not readily apparent, though small cusps are visible.

The presence of the chaotic region can be understood by examining the motion of the physical rod and of the regular islands visible in Fig. 7(b). These regular islands are the ghost rods that we use to explain the topological properties of the homeomorphism φ induced by the rod motion, as analyzed in Ref. [7]. The braid formed by the rod and the ghost rods is $\sigma_1\sigma_2\sigma_3\sigma_2^3\sigma_3^2\sigma_4\sigma_2\sigma_3\sigma_2^3$, which can be shown (with software [29], say) to correspond to a pseudo-Anosov isotopy class with a single separatrix on the boundary, as well as two interior 3-pronged singularities. The singularity data is thus $(N_{\text{sep}} = 1, N_3 = 2)$ for $n = 5$ rods — see Table II.

This brings us to our second observation: where is the injection cusp associated with the boundary separatrix, as predicted by the braid? The injection cusp is there, though it is much less evident than those in Figs. 1, 3, and 5. This is because here the separatrix is associated with a hyperbolic fixed point, as opposed to parabolic in the previous cases. An injection cusp near a parabolic point on the boundary has very 'slow' dynamics near the separatrix, meaning that fluid approaches the separatrix very slowly [1]. This makes the

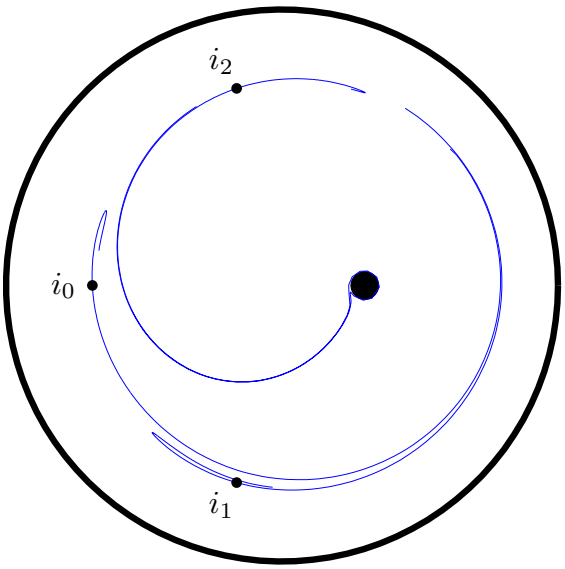

FIG. 8: Portions of the unstable manifold of each iterate of the period-3 hyperbolic orbit near the boundary of the mixing region. The unstable manifold of iterate i_2 enters the mixing region and corresponds to the location of the injection cusp.

separatrices clearly visible as unmixed 'tongues' in Figs. 1, 3, and 5.

In contrast, the injection into the mixing region is governed here by a period-3 hyperbolic orbit near the boundary of the central mixing region. The orbit — consisting of the iterates i_0, i_1, and i_2 — is shown in Fig. 7(a). Notice that the orbit itself does not enter the central mixing region, just as in the cases previously considered the parabolic fixed points at the wall remain there. However, a portion of the unstable manifold of each iterate is shown in Fig. 8: notice how the unstable manifold of iterate i_2 enters the heart of the mixing region, following the rod. This unstable manifold is the boundary separatrix predicted by the braid. Thus, the way in which fluid enters the mixing region is by coming near i_2 and then being dragged along its unstable manifold. The iterates i_0 and i_1 play no role as far as injection into the mixing region is concerned. With hindsight, we can see the unstable manifold of i_2 in the wake of the rod in Fig. 7(a). Because the dynamics in their vicinity is exponential rather than algebraic, hyperbolic injection cusps can dramatically speed up the rate of mixing [30] in the central region. The price to pay is an unmixed region around the wall of the device.

V. DISCUSSION

A stirring device consisting of moving rods undergoing periodic motion induces a mapping of the fluid domain to itself. This mapping can be regarded as a homeomorphism of a punctured surface to itself, where the punctures mimic the moving rods. Having the rods undergo a complex braiding motion guarantees a minimal amount of topological entropy, where by complex we mean that the isotopy class associated with the braid is pseudo-Anosov. The topological entropy is itself a lower bound on the rate of stretching of material lines, a quantity which is important for chaotic mixing.

Topological considerations also predict the nature of the injection of unmixed material into the central mixing region. The number of boundary separatrices in the pseudo-Anosov homeomorphism's unstable foliation determines the number of such injection cusps. The number and position of injection cusps is particularly important for open flows, such as flows in channels, since there the nature of injection has a profound impact on the shape of the downstream mixing pattern (Fig. 2).

Topological index formulas allow us to predict the possible types of unstable foliations that can occur for a fixed number of rods. We did not provide a way of deriving the topological type of the unstable foliation for a given rod stirring protocol. This can be done, for instance, by using an implementation [29] of the Bestvina–Handel algorithm [31]. Using the enumeration presented here, a mixing device can be designed with a specific number of injection cusps into the mixing region, by allowing for enough rods and choosing the appropriate stirring protocol.

More generally, instead of physical rods we can consider periodic orbits associated with a stirring protocol. We call such periodic orbits 'ghost rods' when they play a similar role to physical rods (that is, material lines fold around them as if they were rods) [7, 12, 15, 28, 32]. The topological description presented here applies to the unstable foliation associated with periodic orbits.

In future work, we will consider not just the number of injection cusps, but their relative position as well. Indeed, observe that in Fig 5(b) the position of the injection cusps alternates sides relative to the line of rods. This is thought to be a general feature of pseudo-Anosov stirring protocols, but the proof of this requires careful consideration of whether or not given foliations are *dynamically* allowable, in the sense that they can be realised as the unstable foliation of a pseudo-Anosov homeomorphism.

Acknowledgments

Several of the authors were first introduced to these ideas by Philip Boyland, to whom we are extremely grateful for many stimulating discussions.

[1] E. Gouillart, N. Kuncio, O. Dauchot, B. Dubrulle, S. Roux, and J.-L. Thiffeault, 'Walls inhibit chaotic mixing,' *Phys. Rev. Lett.* **99**, 114501 (2007).

[2] H. Aref, 'Stirring by chaotic advection,' *J. Fluid Mech.* **143**, 1–21 (1984).

[3] H. Aref, 'The development of chaotic advection,' *Phys. Fluids* **14** (4), 1315–1325 (2002).

[4] A. Fathi, F. Laundenbach, and V. Poénaru, 'Travaux de Thurston sur les surfaces,' *Astérisque* **66-67**, 1–284 (1979).

[5] W. P. Thurston, 'On the geometry and dynamics of diffeomorphisms of surfaces,' *Bull. Am. Math. Soc.* **19**, 417–431 (1988).

[6] P. L. Boyland, H. Aref, and M. A. Stremler, 'Topological fluid mechanics of stirring,' *J. Fluid Mech.* **403**, 277–304 (2000).

[7] E. Gouillart, M. D. Finn, and J.-L. Thiffeault, 'Topological mixing with ghost rods,' *Phys. Rev. E* **73**, 036311 (2006).

[8] P. L. Boyland, M. A. Stremler, and H. Aref, 'Topological fluid mechanics of point vortex motions,' *Physica D* **175**, 69–95 (2003).

[9] A. Vikhansky, 'Chaotic advection of finite-size bodies in a cavity flow,' *Phys. Fluids* **15** (7), 1830–1836 (2003).

[10] M. D. Finn, S. M. Cox, and H. M. Byrne, 'Topological chaos in inviscid and viscous mixers,' *J. Fluid Mech.* **493**, 345–361 (2003).

[11] M. D. Finn, S. M. Cox, and H. M. Byrne, 'Chaotic advection in a braided pipe mixer,' *Phys. Fluids* **15** (11), L77–L80 (2003).

[12] J.-L. Thiffeault, 'Measuring topological chaos,' *Phys. Rev. Lett.* **94** (8), 084502 (2005).

[13] J.-L. Thiffeault and M. D. Finn, 'Topology, braids, and mixing in fluids,' *Phil. Trans. R. Soc. Lond. A* **364**, 3251–3266 (2006).

[14] T. Kobayashi and S. Umeda, 'Realizing pseudo-Anosov egg beaters with simple mecanisms,' in *Proceedings of the International Workshop on Knot Theory for Scientific Objects, Osaka, Japan*, 97–109 (Osaka Municipal Universities Press, 2007).

[15] B. J. Binder and S. M. Cox, 'A mixer design for the pigtail braid,' *Fluid Dyn. Res.* **49**, 34–44 (2008).

[16] M. D. Finn, J.-L. Thiffeault, and E. Gouillart, 'Topological chaos in spatially periodic mixers,' *Physica D* **221** (1), 92–100 (2006).

[17] M. D. Finn and J.-L. Thiffeault, 'Topological entropy of braids on the torus,' *SIAM J. Appl. Dyn. Syst.* **6**, 79–98 (2007).

[18] S. C. Jana, G. Metcalfe, and J. M. Ottino, 'Experimental and computational studies of mixing in complex Stokes flows: the vortex mixing flow and multicellular cavity flow,' *J. Fluid Mech.* **269**, 199–246 (1994).

[19] J. S. Birman, *Braids, Links, and Mapping Class Groups*, Annals of Mathematics Studies (Princeton University Press, Princeton, NJ, 1975).

[20] M. Handel, 'Global shadowing of pseudo-Anosov homeomorphisms,' *Ergod. Th. Dynam. Syst.* **8**, 373–377 (1985).

[21] P. L. Boyland, 'Isotopy stability of dynamics on surfaces,' in *Geometry and Topology in Dynamics (Winston-Salem, NC, 1998/San Antonio, TX, 1999)*, *Contemp. Math.*, volume 246, 17–45 (American Mathematical Society, Providence, RI, 1999).

[22] V. I. Arnold and A. Avez, *Ergodic Problems of Classical Mechanics* (W. A. Benjamin, New York, 1968).

[23] R. C. Penner and J. L. Harer, *Combinatorics of Train Tracks*, number 125 in Annals of Mathematics Studies (Princeton University Press, Princeton, NJ, 1991).

[24] G. Band and P. L. Boyland, 'The Burau estimate for the entropy of a braid,' *Algeb. Geom. Topology* **7**, 1345–1378 (2007).

[25] J. W. Milnor, *Topology from the Differentiable Viewpoint*, revised edition (Princeton University Press, Princeton, NJ, 1997).

[26] W. P. Thurston, *Three-dimensional geometry and topology*, volume 1 (Princeton University Press, Princeton, NJ, 1997), edited by Silvio Levy.

[27] G. E. Andrews, *The Theory of Partitions* (Addison-Wesley, Reading, Mass., 1976).

[28] M. A. Stremler and J. Chen, 'Generating topological chaos in lid-driven cavity flow,' *Phys. Fluids* **19**, 103602 (2007).

[29] T. Hall, '*Train: A C++ program for computing train tracks of surface homeomorphisms*,' `http://www.liv.ac.uk/maths/PURE/MIN_SET/CONTENT/members/T_Hall.html`.

[30] E. Gouillart, *Chaotic mixing by rod-stirring devices in open and closed flows*, Ph.D. thesis, Université Pierre et Marie Curie Paris 6 (2007), http://tel.archives-ouvertes.fr/tel-00204109/en.

[31] M. Bestvina and M. Handel, 'Train-tracks for surface homeomorphisms,' *Topology* **34** (1),

109–140 (1995).

[32] J.-L. Thiffeault, E. Gouillart, and M. D. Finn, 'The size of ghost rods,' (2005), arXiv:nlin/0507076.